LETTER

doi:10.1038/nature13896

mTORC1–mediated translational elongation limits intestinal tumour initiation and growth

William J. Faller[1], Thomas J. Jackson[2]*, John R. P. Knight[2]*, Rachel A. Ridgway[1], Thomas Jamieson[1], Saadia A. Karim[1], Carolyn Jones[2], Sorina Radulescu[1], David J. Huels[1], Kevin B. Myant[1], Kate M. Dudek[2], Helen A. Casey[1], Alessandro Scopelliti[1], Julia B. Cordero[1], Marcos Vidal[1], Mario Pende[3], Alexey G. Ryazanov[4], Nahum Sonenberg[5], Oded Meyuhas[6], Michael N. Hall[7], Martin Bushell[2], Anne E. Willis[2] & Owen J. Sansom[1]

Inactivation of APC is a strongly predisposing event in the development of colorectal cancer[1,2], prompting the search for vulnerabilities specific to cells that have lost APC function. Signalling through the mTOR pathway is known to be required for epithelial cell proliferation and tumour growth[3–5], and the current paradigm suggests that a critical function of mTOR activity is to upregulate translational initiation through phosphorylation of 4EBP1 (refs 6, 7). This model predicts that the mTOR inhibitor rapamycin, which does not efficiently inhibit 4EBP1 (ref. 8), would be ineffective in limiting cancer progression in APC-deficient lesions. Here we show in mice that mTOR complex 1 (mTORC1) activity is absolutely required for the proliferation of *Apc*-deficient (but not wild-type) enterocytes, revealing an unexpected opportunity for therapeutic intervention. Although APC-deficient cells show the expected increases in protein synthesis, our study reveals that it is translation elongation, and not initiation, which is the rate-limiting component. Mechanistically, mTORC1-mediated inhibition of eEF2 kinase is required for the proliferation of APC-deficient cells. Importantly, treatment of established APC-deficient adenomas with rapamycin (which can target eEF2 through the mTORC1–S6K–eEF2K axis) causes tumour cells to undergo growth arrest and differentiation. Taken together, our data suggest that inhibition of translation elongation using existing, clinically approved drugs, such as the rapalogs, would provide clear therapeutic benefit for patients at high risk of developing colorectal cancer.

The ability of the intestinal epithelium to regenerate after challenge has been well described[9–11]. We have shown that this is a Wnt-driven process that mimics the proliferation observed after *Apc* deletion[11,12] and is a valuable model of the early stages of intestinal cancer. However, the underlying mechanisms controlling these processes are largely unknown. The serine/threonine kinase mTOR, particularly as part of mTORC1, is a known mediator of cell growth and proliferation[13]. Previous studies have suggested that mTORC1 may be important in both the intestinal stem-cell niche and for intestinal tumorigenesis[4,5,14]. We therefore queried the role of mTORC1 in intestinal proliferation after Wnt activation. Following *Apc* deletion there was an increase in the phosphorylation status of the mTORC1 effectors RPS6 and 4EBP1 that was dependent on MYC expression. Increased phosphorylation of these proteins was also seen during crypt regeneration (Fig. 1a–c and Extended Data Fig. 1a). Importantly, the mTOR inhibitor rapamycin blocked intestinal regeneration, demonstrating that mTOR signalling is required for this process (Fig. 1d, e). Given that rapamycin did not affect apoptosis or proliferation in the normal intestine (Extended Data Fig. 1b, c), these data suggest that there may be a potential therapeutic window, between normal intestinal enterocytes and those with a high level of Wnt activity. Therefore, we deleted raptor (*Rptor*; an essential component of mTORC1) in

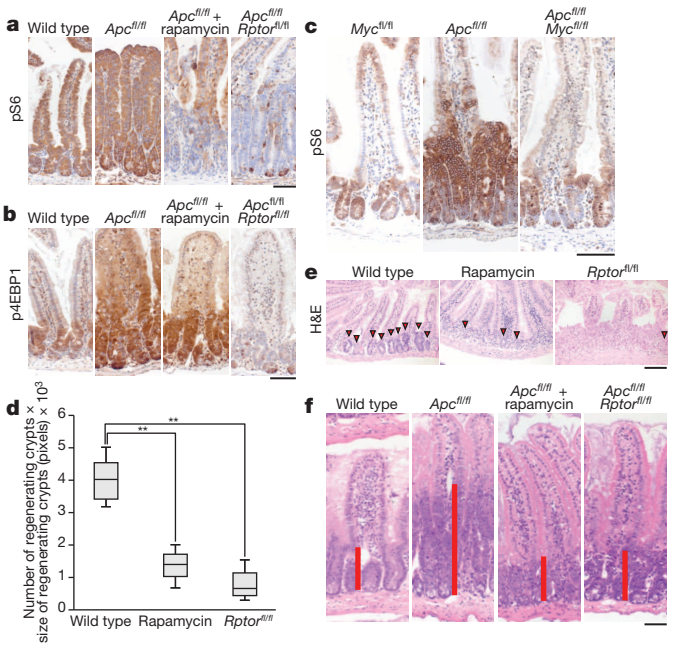

Figure 1 | mTORC1 is essential for Wnt-driven proliferation in a MYC-dependent manner. **a**, **b**, Representative immunohistochemistry (IHC) of phospho-RPS6 (pS6) and phospho-4EBP1 (p4EBP1) showing increased staining 96 h after *Apc* deletion. *Rptor* deletion caused a loss of positivity in both, whereas 10 mg kg^{-1} rapamycin treatment (beginning at 24 h) specifically disrupts RPS6 phosphorylation (representative of six biological replicates). **c**, Representative IHC of phospho-RPS6 96 h after Cre induction showing that Wnt-driven RPS6 phosphorylation is MYC dependent (representative of 3 biological replicates). **d**, Mice were exposed to 14 Gy γ-irradiation and intestinal regeneration was measured 72 h later by counting the number of viable crypts and multiplying that by the average size of the regenerating crypts. Boxplot shows that 10 mg kg^{-1} rapamycin treatment and *Rptor* deletion significantly decrease intestinal regeneration. Whiskers show maximum and minimum, black line shows median ($n = 6$ biological replicates per group). $^{**}P$ value < 0.02, Mann–Whitney U test. **e**, Representative haematoxylin and eosin (H&E) staining of regenerating intestines 72 h after exposure to 14 Gy γ-irradiation. Arrowheads indicate regenerating crypts (representative of 6 biological replicates). **f**, Representative H&E staining 96 h after *Apc* loss, showing that 10 mg kg^{-1} rapamycin treatment or *Rptor* deletion prevent Wnt-driven proliferation (representative of 6 biological replicates). Treatment began 24 h after *Apc* deletion. Red bar is graphical representation of crypt size. Scale bars, 100 μm.

[1]Cancer Research UK Beatson Institute, Glasgow G61 1BD, UK. [2]Medical Research Council Toxicology Unit, Leicester LE1 9HN, UK. [3]Institut Necker-Enfants Malades, CS 61431, Paris, France Institut National de la Santé et de la Recherche Médicale, U1151, F-75014 Paris, France Université Paris Descartes, Sorbonne Paris Cité, 75006 Paris, France. [4]Department of Pharmacology, Rutgers The State University of New Jersey, Robert Wood Johnson Medical School, Piscataway, New Jersey 08854, USA. [5]Department of Biochemistry and Goodman Cancer Research Center, McGill University, Montreal, Québec H3A 1A3, Canada. [6]Department of Biochemistry and Molecular Biology, IMRIC, The Hebrew University-Hadassah Medical School, Jerusalem 91120, Israel. [7]Biozentrum, University of Basel, CH-4056 Basel, Switzerland.

*These authors contributed equally to this work.

the intestinal epithelium (Extended Data Fig. 1d). Surprisingly, normal gut homeostasis was unaffected by raptor loss 4 days after Cre induction, when using an epithelium-specific Cre-recombinase (*VillinCre*^{ER} *Rptor*$^{fl/fl}$) (Extended Data Fig. 1e, f). Furthermore, 400 days after induction, no phosphorylation of RPS6 or 4EBP1 was observed, showing that *Rptor* deletion was sustained (Extended Data Fig. 2a). Raptor loss caused no change in levels of either mitosis or apoptosis (Extended Data Fig. 2b, c) but proved to be essential for the proliferative phenotype observed during regeneration or after *Apc* deletion (Fig. 1a, b, d–f). Nuclear localization of β-catenin and high levels of MYC could be demonstrated by immunohistochemistry (IHC), showing that Wnt activation is still present (Extended Data Fig. 3a, b).

Given that rapamycin treatment and *Rptor* deletion had similar effects, we examined whether rapamycin treatment was sufficient to modify intestinal tumorigenesis, either prophylactically or chemotherapeutically. First we assessed whether rapamycin could suppress a model of intestinal tumorigenesis, in which *Apc* deletion is targeted to Lgr5-positive stem cells using *Lgr5Cre*^{ER} (*Lgr5Cre*^{ER} *Apc*$^{fl/fl}$). Mice were treated starting 10 days after Cre induction and, in contrast to controls, remained tumour free for the duration of the experiment (Fig. 2a, b). Next we treated mice (*Apc*$^{Min/+}$ or *LGR5Cre*^{ER} *Apc*$^{fl/fl}$) with established adenomas. Remarkably, the mice lost their clinical symptoms of disease and survived significantly

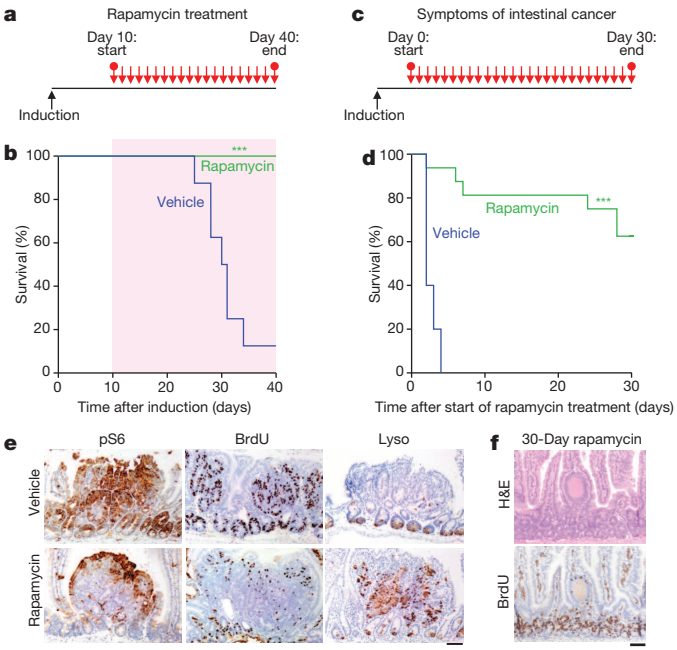

Figure 2 | Tumorigenesis driven by the loss of *Apc* requires mTORC1 activation. **a**, **b**, Graphical representation of prophylactic rapamycin treatment strategy and Kaplan–Meyer survival curve showing that prophylactic rapamycin treatment prevents tumorigenesis. Rapamycin treatment (10 mg kg^{-1}) began at day 10 after *Apc* deletion, and lasted 30 days, after which mice were sampled. Area highlighted by red indicates duration of rapamycin treatment ($n = 8$, vehicle; $n = 13$, rapamycin). ***P value ≤ 0.001, log-rank test. **c**, **d**, Graphical representation of chemotherapeutic rapamycin treatment strategy and Kaplan–Meyer survival curve showing that rapamycin treatment can regress established intestinal tumours. Rapamycin treatment (10 mg kg^{-1}) started when mice showed signs of intestinal disease, and lasted 30 days, after which mice were sampled. Graph represents survival while on rapamycin treatment ($n = 5$, vehicle; $n = 16$, rapamycin). ***P value ≤ 0.001, log-rank test. **e**, Representative IHC of phospho-RPS6, 5-bromodeoxyuridine (BrdU) and lysozyme (Lyso), showing that 72 h of 10 mg kg^{-1} rapamycin treatment causes a loss in RPS6 phosphorylation and BrdU positivity, and an increase in lysozyme staining in intestinal tumours (representative of 5 biological replicates). **f**, Representative H&E staining and IHC for BrdU showing that small, non-proliferative lesions remain after 30 days of 10 mg kg^{-1} rapamycin treatment (representative of 5 biological replicates). Scale bars, 100 μm.

longer than controls (Fig. 2c, d and Extended Data Fig. 3c). We next analysed the tumours from these mice over a time course after rapamycin treatment. Treatment caused a loss of proliferation specifically within the tumours by 72 h, and an increase in the number of lysozyme-positive Paneth cells (Fig. 2e and Extended Data Fig. 3d, e). By 30 days, most tumours had shrunk considerably to small non-proliferative lesions that no longer contained Paneth cells (Fig. 2f and Extended Data Fig. 3f). Within the normal intestine there are two main cell populations that show high levels of Wnt signalling; the label-retaining/progenitor population and the Paneth cell population[15]. Our data suggest that treatment of mice with rapamycin causes the differentiation of the tumour's Wnt-high progenitor cells into the other Wnt-high fate in the intestine: namely non-proliferative Paneth-like cells. The cell-cycle arrest in these cells was examined by staining for p21, p16 and p53. No increase in these markers was observed, suggesting that a classical cell-cycle arrest pathway had not been engaged (Extended Data Fig. 4a). We reasoned that if mice were removed from rapamycin the tumours would regain proliferative capacity. Indeed, when rapamycin treatment was halted, signs of intestinal neoplasia were observed approximately 40–60 days later (Extended Data Fig. 3c). This suggested that intestinal adenoma stem cells were still present. Tumours from *Lgr5GFPCre*^{ER} mice were stained to detect LGR5–GFP positivity. We found that, after rapamycin treatment, numerous LGR5-positive cells were still present, indicating that, although rapamycin treatment causes a regression of the lesions, the tumour-initiating cells remain (Extended Data Fig. 4b).

We next examined the mechanism of mTORC1 requirement after *Apc* loss. mTORC1 is known to regulate protein synthesis on multiple levels and most research has focused on two downstream effectors: 4EBP1 and S6K. A number of studies have suggested that translation initiation, via the 4EBP1–eIF4E axis, is the critical effector of mTOR in cancer[6,16]. However, it has been shown that rapamycin preferentially inhibits the phosphorylation of S6K over 4EBP1 (ref. 8), suggesting that 4EBP1-mediated inhibition of translation initiation may not be limiting in the context of *Apc* loss. To assess the changes in translational control in response to mTORC1 inhibition, we measured the polysomal distribution in wild-type, *Apc*-deficient and *Apc/Rptor*-deficient intestinal epithelial cells 4 days after gene deletion. *Apc* deletion resulted in a decrease in the number of polysomes, whereas *Apc/Rptor* co-deletion reversed this effect (Fig. 3a). The decrease in the number of polysomes after *Apc* deletion could suggest either reduced translation initiation (and, consequently, a lower overall level of translation) and/or a faster rate of translational elongation. Global translation rates were measured using an *in vitro* intestinal crypt culture model[17]. The *Apc*-deficient cells were shown to have increased ^{35}S-labelled methionine/cysteine incorporation compared with wild type, showing higher overall levels of protein synthesis (Fig. 3b). Unfortunately, *Rptor* deletion prevented the growth of crypts *in vitro* so this could not be assayed (Extended Data Fig. 5).

To measure the rate of translational elongation, an *in vitro* harringtonine run-off assay was performed[18], as described in Methods. There was a >2.5-fold increase in ribosome run-off in crypts with *Apc* deletion compared with wild type (Fig. 3c and Extended Data Fig. 6a–d). This suggests that, after Wnt activation, elongation, rather than initiation, is rate limiting for protein synthesis and that mTORC1 must be activated to overcome this.

Cycloheximide (an inhibitor of elongation[19]) reduced proliferation associated with *Apc* deletion to a similar level to rapamycin (Extended Data Fig. 6e, f). While cycloheximide is acknowledged to inhibit elongation[19], it must be emphasized that 72 h treatment could result in broad alterations in protein synthesis. However, the *Apc*$^{fl/fl}$-specific loss of proliferation observed here provides 'proof of principle' to demonstrate that the modulation of protein synthesis may be useful as a chemotherapeutic strategy.

As most previous work has suggested that translation initiation downstream of 4EBP1 is limiting to cancer[20], it was important to probe known effectors of mTORC1 in this system. Given the alteration of elongation rates, eEF2K, a known target of S6K[21,22] was of particular interest. eEF2K

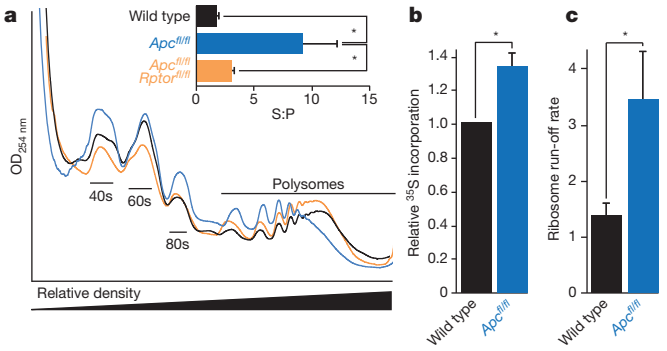

Figure 3 | mTORC1 drives increased translational elongation. **a**, Representative polysome profiles of intestinal epithelial cells showing altered RNA distribution 96 h after *Apc* deletion. Bar graph represents the ratio of sub-polysomes compared with polysomes (S:P). $OD_{254\,nm}$, optical density at 254 nm. Data are average ± standard error of the mean (s.e.m.) ($n = 3$ per group). *P value ≤ 0.05, Mann–Whitney U test. **b**, Intestinal crypt culture was pulsed for 30 min with ^{35}S-labelled methionine/cysteine. Incorporation of ^{35}S into protein was quantified by scintillation counting and normalized to total protein. *Apc* deletion increases ^{35}S incorporation. Data are average ± s.e.m. ($n = 3$ biological replicates per group). *P value ≤ 0.05, Mann–Whitney U test. **c**, The ribosome run-off rate was measured by addition of the initiation inhibitor harringtonine to *ex vivo* crypts from wild-type and *Apc*-deleted mice. Harringtonine was added for 0 or 180 s and the increase in sub-polysomes relative to polysomes was calculated. This run-off rate represents the shift in S:P between the two time points, which is proportional to elongation speed. Data are average ± s.e.m. ($n = 3$ biological replicates per group). *P value ≤ 0.05, Mann–Whitney U test. Also see Extended Data Fig. 6.

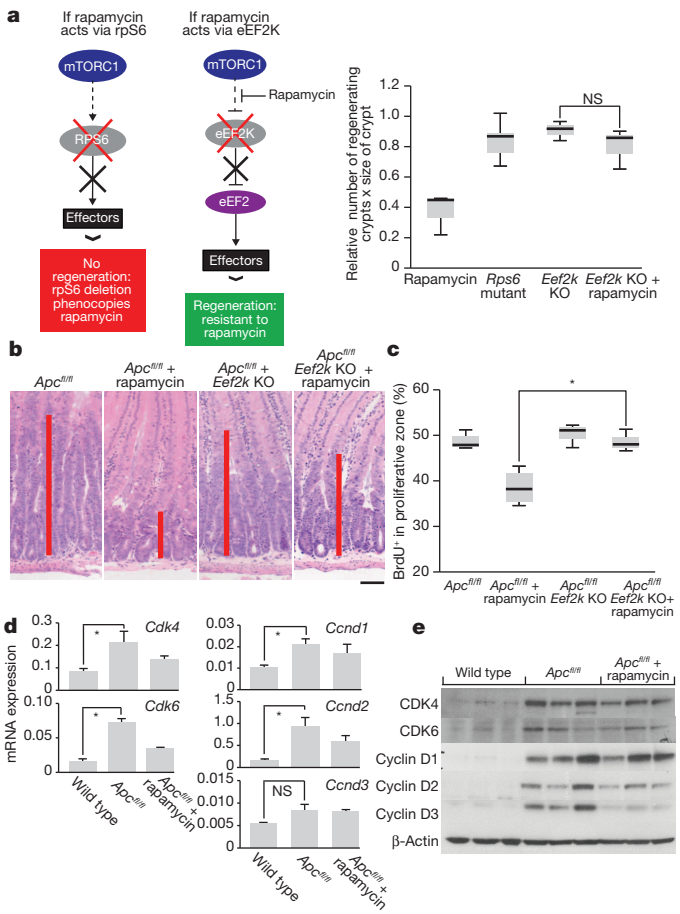

Figure 4 | mTORC1 signalling via eEF2K controls intestinal proliferation after Wnt signalling. **a**, Graphical representation of findings and boxplots showing that murine intestinal regeneration after irradiation implicates the mTORC1–S6K–eEF2K axis in Wnt-driven proliferation. Mice were exposed to 14 Gy γ-irradiation, and intestinal regeneration was calculated 72 h after exposure by examining the number and size of regenerating crypts relative to wild-type regenerating intestines. KO, knockout. Whiskers show maximum and minimum, black line shows median ($n = 6$ per group). *P value ≤ 0.05, Mann–Whitney U test. NS, not significant. **b**, **c**, Representative H&E and boxplot showing that *Eef2k* deletion confers resistance to 10 mg kg^{-1} rapamycin treatment, 96 h after *Apc* deletion. Treatment began 24 h after induction. Red bar is graphical representation of crypt size. Whiskers show maximum and minimum, black line shows median ($n = 3$ biological replicates per group). *P value < 0.05, Mann–Whitney U test. Scale bar, 100 μm. **d**, Polymerase chain reaction with quantitative reverse transcription (qRT–PCR) of intestinal epithelial cells using primers for *Cdk4*, *Cdk6*, *Ccnd1*, *Ccnd2* and *Ccnd3*. *Ccnd3* is not regulated at the transcriptional level. Data were normalized to *Gapdh*. Data are average ± s.e.m. ($n = 3$ biological replicates per group). *P value ≤ 0.05, Mann–Whitney U test. NS, not significant. **e**, Western blot analysis of intestinal epithelial cells from each group. Antibodies to CDK4, CDK6, cyclin D1, cyclin D2, cyclin D3 and β-actin are shown. Each well represents a different mouse from the relevant group, and the samples are the same as those used for the qRT–PCR.

is a negative regulator of eEF2, giving mTORC1 the ability to promote translational elongation via S6K (ref. 23). Using multiple mouse knockout and knock-in alleles, we further dissected the downstream effectors of mTORC1 in intestinal regeneration. *S6k1/2* (also known as *Rps6kb1* and *Rps6kb2*, respectively) knockout decreased intestinal regeneration, while knockout of *Eif4ebp1/2* (coding 4EBP1 and 4EBP2, respectively) had no effect. As the 4EBP proteins are negative regulators of eIF4E, an increase (rather than a decrease) in regeneration may have been predicted, but this was not found. Moreover these intestines were still sensitive to rapamycin, demonstrating that rapamycin was acting via the mTORC1–S6K branch rather than the 4EBP1–eIF4E branch (Extended Data Fig. 7). We then used an *Eef2k*-null mouse and showed that after irradiation and treatment with rapamycin, these mice were now resistant to mTORC1 inhibition, confirming the importance of translational elongation (Fig. 4a). To ensure that S6K was not also acting through its more established effector, rpS6, we used an *Rps6* phospho-mutant that cannot be phosphorylated by S6K. This was unable to phenocopy *Rptor* deletion (Fig. 4a), showing that Wnt-driven regeneration requires increased translational elongation, mediated through mTORC1.

To prove that inhibition of eEF2K by S6K is required to allow increased eEF2 activity after *Apc* loss, we intercrossed *VillinCre*^{ER} *Apc*$^{fl/fl}$ to *Eef2k*$^{-/-}$ mice and treated these with rapamycin. In contrast to *VillinCre*^{ER} *Apc*$^{fl/fl}$ mice, these intestines were now resistant to the growth inhibitory effects of rapamycin (Fig. 4b, c). Tellingly, these mice no longer show an increase in the inhibitory phosphorylation of eEF2 after rapamycin treatment (Extended Data Fig. 8).

To assess whether the increased elongation after *Apc* deletion had differential effects on cell-cycle-regulating proteins, RNA and protein levels of several key cell-cycle regulators were tested (Fig. 4d, e). This analysis revealed that while there were increased RNA and protein levels of cyclin D1, cyclin D2, CDK4 and CDK6, cyclin D3 had increased protein levels in the absence of increased messenger RNA levels. Cyclin D3 protein levels were sensitive to rapamycin exposure, and this sensitivity depends on eEF2K (Extended Data Fig. 9). Additionally, ribosomes were shown to elongate approximately four times faster on cyclin D3 messages in *Apc*-deficient cells than in wild-type cells. No differences were detected in other messages tested (Extended Data Fig. 10). Taken together, these data suggest that cyclin D3 is translationally regulated at the level of elongation, consistent with previous reports[24,25]. The contribution of cyclin D3 to the proliferative phenotype remains to be elucidated.

We report that mTORC1 is an essential downstream effector of Wnt signalling in the intestine. We show that intestinal proliferation associated with Wnt signalling requires the mTORC1–S6K–eEF2K–eEF2 axis, and that the resulting increase in the rate of elongation of specific polypeptides overcomes a limiting translational step. Our work highlights key functional roles for eEF2K and translational elongation in the control of the initiation of cancer and adenomatous proliferation. The

importance of elongation in this context has been suggested in a small number of publications, but this study provides key *in vivo* evidence[26–28]. Finally, we have also shown that targeting mTOR and translational control may be a viable strategy for chemoprevention of colorectal carcinoma in high-risk patients, and treatment of early stage disease. Indeed, recent studies have suggested that the chemopreventative agents aspirin and mesalazine also target mTOR[29,30].

Online Content Methods, along with any additional Extended Data display items and Source Data, are available in the online version of the paper; references unique to these sections appear only in the online paper.

Received 4 October 2013; accepted 26 September 2014.
Published online 5 November 2014.

1. Kinzler, K. W. & Vogelstein, B. Lessons from hereditary colorectal cancer. *Cell* **87,** 159–170 (1996).
2. Korinek, V. *et al.* Constitutive transcriptional activation by a beta-catenin-Tcf complex in $APC^{-/-}$ colon carcinoma. *Science* **275,** 1784–1787 (1997).
3. Ashton, G. H. *et al.* Focal adhesion kinase is required for intestinal regeneration and tumorigenesis downstream of Wnt/c-Myc signaling. *Dev. Cell* **19,** 259–269 (2010).
4. Fujishita, T., Aoki, K., Lane, H. A., Aoki, M. & Taketo, M. M. Inhibition of the mTORC1 pathway suppresses intestinal polyp formation and reduces mortality in $Apc^{\Delta 716}$ mice. *Proc. Natl Acad. Sci. USA* **105,** 13544–13549 (2008).
5. Gulhati, P. *et al.* Targeted inhibition of mammalian target of rapamycin signaling inhibits tumorigenesis of colorectal cancer. *Clin. Cancer Res.* **15,** 7207–7216 (2009).
6. Pourdehnad, M. *et al.* Myc and mTOR converge on a common node in protein synthesis control that confers synthetic lethality in Myc-driven cancers. *Proc. Natl Acad. Sci. USA* **110,** 11988–11993 (2013).
7. Martineau, Y. *et al.* Pancreatic tumours escape from translational control through 4E-BP1 loss. *Oncogene* **33,** 1367–1374 (2014).
8. Jiang, Y. P., Ballou, L. M. & Lin, R. Z. Rapamycin-insensitive regulation of 4E-BP1 in regenerating rat liver. *J. Biol. Chem.* **276,** 10943–10951 (2001).
9. Bach, S. P., Renehan, A. G. & Potten, C. S. Stem cells: the intestinal stem cell as a paradigm. *Carcinogenesis* **21,** 469–476 (2000).
10. Bernal, N. P. *et al.* Evidence for active Wnt signaling during postresection intestinal adaptation. *J. Pediatr. Surg.* **40,** 1025–1029 (2005).
11. Ireland, H. *et al.* Inducible Cre-mediated control of gene expression in the murine gastrointestinal tract: effect of loss of β-catenin. *Gastroenterology* **126,** 1236–1246 (2004).
12. Muncan, V. *et al.* Rapid loss of intestinal crypts upon conditional deletion of the Wnt/Tcf-4 target gene c-*Myc*. *Mol. Cell. Biol.* **26,** 8418–8426 (2006).
13. Zoncu, R., Efeyan, A. & Sabatini, D. M. mTOR: from growth signal integration to cancer, diabetes and ageing. *Nature Rev. Mol. Cell Biol.* **12,** 21–35 (2011).
14. Yilmaz, Ö. H. *et al.* mTORC1 in the Paneth cell niche couples intestinal stem-cell function to calorie intake. *Nature* **486,** 490–495 (2012).
15. Farin, H. F., Van Es, J. H. & Clevers, H. Redundant sources of Wnt regulate intestinal stem cells and promote formation of Paneth cells. *Gastroenterology* **143,** 1518–1529 (2012).
16. She, Q. B. *et al.* 4E-BP1 is a key effector of the oncogenic activation of the AKT and ERK signaling pathways that integrates their function in tumors. *Cancer Cell* **18,** 39–51 (2010).
17. Sato, T. *et al.* Single Lgr5 stem cells build crypt–villus structures *in vitro* without a mesenchymal niche. *Nature* **459,** 262–265 (2009).
18. Fresno, M., Jimenez, A. & Vazquez, D. Inhibition of translation in eukaryotic systems by harringtonine. *Eur. J. Biochem.* **72,** 323–330 (1977).
19. Schneider-Poetsch, T. *et al.* Inhibition of eukaryotic translation elongation by cycloheximide and lactimidomycin. *Nature Chem. Biol.* **6,** 209–217 (2010).
20. Hsieh, A. C. *et al.* The translational landscape of mTOR signalling steers cancer initiation and metastasis. *Nature* **485,** 55–61 (2012).
21. Richter, J. D. & Sonenberg, N. Regulation of cap-dependent translation by eIF4E inhibitory proteins. *Nature* **433,** 477–480 (2005).
22. Browne, G. J. & Proud, C. G. A novel mTOR-regulated phosphorylation site in elongation factor 2 kinase modulates the activity of the kinase and its binding to calmodulin. *Mol. Cell. Biol.* **24,** 2986–2997 (2004).
23. Ryazanov, A. G., Shestakova, E. A. & Natapov, P. G. Phosphorylation of elongation factor 2 by EF-2 kinase affects rate of translation. *Nature* **334,** 170–173 (1988).
24. Gorshtein, A. *et al.* Mammalian target of rapamycin inhibitors rapamycin and RAD001 (everolimus) induce anti-proliferative effects in GH-secreting pituitary tumor cells *in vitro*. *Endocr. Relat. Cancer* **16,** 1017–1027 (2009).
25. Gutzkow, K. B. *et al.* Cyclic AMP inhibits translation of cyclin D3 in T lymphocytes at the level of elongation by inducing eEF2-phosphorylation. *Cell. Signal.* **15,** 871–881 (2003).
26. Firczuk, H. *et al.* An *in vivo* control map for the eukaryotic mRNA translation machinery. *Mol. Syst. Biol.* **9,** 635 (2013).
27. Hussey, G. S. *et al.* Identification of an mRNP complex regulating tumorigenesis at the translational elongation step. *Mol. Cell* **41,** 419–431 (2011).
28. Nakamura, J. *et al.* Overexpression of eukaryotic elongation factor eEF2 in gastrointestinal cancers and its involvement in G2/M progression in the cell cycle. *Int. J. Oncol.* **34,** 1181–1189 (2009).
29. Din, F. V. *et al.* Aspirin inhibits mTOR signaling, activates AMP-activated protein kinase, and induces autophagy in colorectal cancer cells. *Gastroenterology* **142,** 1504–1515 (2012).
30. Baan, B. *et al.* 5-Aminosalicylic acid inhibits cell cycle progression in a phospholipase D dependent manner in colorectal cancer. *Gut* **61,** 1708–1715 (2012).

Acknowledgements W.J.F. is funded by AICR. O.J.S. is funded by Cancer Research UK, European Research Council Investigator Grant (COLONCAN) and the European Union Seventh Framework Programme FP7/2007-2013 under grant agreement number 278568. M.B. is a Medical Research Council Senior Fellow. The authors acknowledge P. Cammareri, J. Morton and C. Murgia for proofreading of the manuscript.

Author Contributions O.J.S., A.E.W. and W.J.F. designed the project. W.J.F., R.A.R., T.J. and S.R. performed breeding and phenotypic analysis of mice; W.J.F., T.J.J. and J.R.P.K. performed translational analysis; M.N.H., A.G.R., N.S., O.M., A.S., J.B.C., M.V., D.J.H., K.B.M., S.A.K., K.M.D., C.J., H.A.C. and M.P. provided advice and material; W.J.F., O.J.S., A.E.W. and M.B. wrote and edited the manuscript.

Author Information Reprints and permissions information is available at www.nature.com/reprints. The authors declare no competing financial interests. Readers are welcome to comment on the online version of the paper. Correspondence and requests for materials should be addressed to O.J.S. (o.sansom@beatson.gla.ac.uk).

METHODS

Mouse colonies. All experiments were performed according with UK Home Office regulations (licence 60/4183) which undergoes local ethical review at Glasgow University. Outbred male mice from 6 to 12 weeks of age were used. The majority of the work was performed on C57BL/6 mice: *AhCre*, $Apc^{fl/fl}$, $Apc^{Min/+}$, $Rptor^{fl/fl}$, *S6k1/2* knockout and $Rps6^{mut}$ mice were all C57BL/6J. Some treatment experiments were performed on mice that were only three generations C57BL/6 ($Lgr5Cre^{ER}$ $Apc^{fl/fl}$).

The alleles used were as follows: $VillinCre^{ER}$ (ref. 31). *AhCre* (ref. 11), $Lgr5Cre^{ER}$ (ref. 32), Apc^{580} (ref. 33), $Apc^{Min/+}$ (ref. 34), $Myc^{fl/fl}$ (ref. 35), $Rptor^{fl/fl}$ (ref. 36), *ROSA-tdRFP* (ref. 37), *Eif4ebp1* knockout (ref. 38), *Eif4ebp2* knockout (ref. 39), *S6k1* knockout (ref. 40), *S6k2* knockout (ref. 41), *Eef2k* knockout (ref. 42), $Rps6^{mut}$ (ref. 43). Recombination by $VillinCre^{ER}$ was induced with one intraperitoneal (i.p.) injection of 80 mg kg^{-1} tamoxifen on day 0 and day 1. Analysis of $VillinCre^{ER}$-induced mice was at day 4 after induction. Red fluorescent protein (RFP) analysis was carried out by inducing recombination by *AhCre* using a single i.p. injection of 80 mg kg^{-1} β-napthoflavone. RFP visualization was carried out on day 4. Mice carrying the $Lgr5Cre^{ER}$ transgene were given one i.p. injection of 120 mg kg^{-1} tamoxifen.

For regeneration experiments, mice were exposed to γ-irradiation from caesium-137 sources. This delivered γ-irradiation at 0.423 Gy min^{-1}.

Rapamycin treatment was performed using a daily i.p. injection of 10 mg kg^{-1} (refs 43, 44) in 5% Tween80 and 5% polyethylene glycol in PBS. Cycloheximide treatment was performed using a daily i.p. injection of 35 mg kg^{-1} in PBS.

In accordance with the 3Rs, the smallest sample size was chosen that could give a significant difference. Given the robust phenotype of the $Apc^{fl/fl}$, and our prediction that mTOR was essential, the minimum sample size assuming no overlap in control versus experimental is three animals.

No randomization was used and the experimenter was blinded to drugs and genotypes.

IHC. Standard IHC techniques were used throughout this study. Antibody concentrations used were as follows: phospho-rpS6$^{Ser\,235/236}$ (1:800; Cell Signaling 4858), phospho-4EBP1$^{Thr\,37/46}$ (1:500; Cell Signaling 2855), phospho-eEF2$^{Thr\,56}$ (1:500; Novus Biologicals NB100-92518), c-MYC (1:200; Santa Cruz sc-764), β-catenin (1:50; BD Biosciences 610154), BrdU (1:200; BD Biosciences 347580), lysozyme (1:150; Dako A099), GFP (1:1,000; Abcam ab6556), p21 (1/4; CNIO Madrid), p16 (1:400; Santa Cruz sc1661), p53 (1/150; Vector Laboratories VPP956). For each antibody, staining was performed on at least three mice of each genotype. Representative images are shown for each staining.

Assaying apoptosis, mitosis and proliferation *in vivo*. Apoptosis and mitotic index were scored from H&E-stained sections as previously described[11]. Proliferation levels were assessed by measuring BrdU incorporation. Mice were injected with 250 μl of BrdU (Amersham Biosciences) 2 h before being killed. Immunohistochemical staining for BrdU was then performed using an anti-BrdU antibody. For each analysis, 25 full crypts were scored from at least three mice of each genotype.

Intestinal epithelium extraction. To generate tissue for polysomal profile analysis, 10-cm portions of intestine were flushed with 0.1 mg ml^{-1} cycloheximide (Sigma) in PBS and inverted over a glass rod to expose the epithelial surface. Intestines were incubated in 0.1 mg ml^{-1} cycloheximide in HBSS (Gibco) with 10 mM EDTA for 5 min at 37 °C followed by 5 min of vigorous shaking. Intestines were transferred to 0.1 mg ml^{-1} cycloheximide in PBS and incubated for a further 5 min at 4 °C, followed by 5 min of vigorous shaking. This fraction contained intestinal crypts and was used for downstream analysis.

Sucrose density ultracentrifugation. Intestinal epithelial cells were lysed in ice-cold 300 mM NaCl, 15 mM $MgCl_2$, 15 mM Tris (pH 7.5) containing 500 units ml^{-1} RNAsin, 1 mg ml^{-1} heparin sulphate and 0.1 mg ml^{-1} cycloheximide supplemented with 0.1% (v/v) Triton X-100. Post-nuclear lysates were layered on 10 ml 10–50% (w/v) sucrose gradients of the same buffer omitting Triton X-100. Gradients were centrifuged at 38,000 r.p.m. for 2 h at 4 °C in a SW40Ti rotor (Beckman Coulter) and separated through a live $OD_{254\,nm}$ ultraviolet spectrometer (Isco). Comparison of peak abundance was based on the area under the curve.

Crypt culture. Mouse small intestines were opened longitudinally and washed with PBS. Crypts were isolated as previously described[17]. Isolated crypts were mixed with 50 μl of Matrigel (BD Bioscence), plated in 24-well plates in Advanced DMEM/F12 with Noggin (100 ng ml^{-1}, Peprotech). Wild-type crypts were also supplemented with R-spondin (500 ng ml^{-1}; R&D Systems). Growth factors were added every other day. Sphere formation was scored 7 days after plating, by counting the number of spheres present per well.

Determination of protein synthesis rates. Cells were treated with 30 μCi ml^{-1} ^{35}S-methionine label (Hartmann Analytic) for 30 min then harvested and lysed. Protein was precipitated onto filter paper (Whatmann) by addition of trichloroacetic acid to 12.5% and washed with 70% ethanol then acetone. Scintillation was read from dried filter paper in triplicate for each experimental condition (National Diagnostics). Total protein content was determined by bicinchoninic acid (BCA) assay (Pierce) for standardization between conditions.

Harringtonine run-off assay. Harringtonine inhibits *de novo* translational initiation, allowing ribosomes engaged in elongation to run-off their messages while limiting re-initiation post-termination. Harringtonine was added for 0 or 180 s and the increase in sub-polysomes relative to polysomes was calculated. This run-off rate represents the shift in S:P between the two time points, which is proportional to elongation speed. Crypt cultures were treated with 2 μg ml^{-1} Harringtonine (Insight Biotechnology) and at set time periods (0 and 180 s) 0.1 mg ml^{-1} cycloheximide was added. Cells were scraped into PBS at 4 °C and prepared for sucrose gradient ultracentrifugation as previously described.

Western blotting. Snap-frozen intestinal epithelial tissue (50–100 mg) was homogenized using the Precellys 24 (Stretton Scientific) in 500 μl of Ripa-lysis buffer. Protein concentrations were determined using a BCA Protein Assay Kit (Pierce). Equal amounts of cellular protein (30 μg) were separated on a 4–12% gradient gel (Novex) and subsequently transferred to a PVDF membrane (Amersham). Total protein was visualized with Poinceau (Sigma). After blocking the membranes in TBS containing 5% BSA (Sigma), 0.02% Triton X-100 for 1 h, primary antibodies were added in block solution at the following dilutions: CDK4 (Santa Cruz SC-260, 1:1,000), CDK6 (Cell Signaling 3136, 1:1,000), cyclin D1 (Cell Signaling 2926, 1:2,000), cyclin D2 (Cell Signaling 3741, 1:1,000), cyclin D3 (Cell Signaling 2936, 1:2,000), eEF2K (Cell Signaling 3692, 1:1,000) and β-actin (Sigma A2228, 1:5,000). After washing, the appropriate HRP-conjugated secondary goat antibodies (Dako) were added diluted 1:10,000 in block for 1 h. Antibody binding was detected using ECL Western Blotting Substrate (Pierce). Primary antibody incubations were carried out at 4 °C overnight. Remaining incubations were carried out at room temperature.

RNA isolation. Snap-frozen intestinal epithelial tissue was homogenized and RNA was extracted using the TRIzol method (Ambion).

qPCR. One microgram of RNA was reverse transcribed to cDNA using a Quantitect Reverse Transcription Kit (Qiagen) in a reaction volume of 20 μl. qPCR was performed on each sample in triplicate in a 20 μl reaction mixture containing 10 μl of 2× DyNAmo HS master mix (Thermo Scientific), 0.5 μM of each of the primers (detailed later) and 2 μl cDNA generated previously. The reaction mixture without a template was run in triplicate as a control. The reaction conditions were as follows: 95 °C for 15 min, followed by 40 cycles of three steps consisting of denaturation at 94 °C for 15 s, primer annealing at 60 °C for 30 s, and primer extension at 72 °C for 30 s. A melting curve analysis was performed from 70 °C to 95 °C in 0.3 °C intervals. *Gapdh* was used to normalize for differences in RNA input.

qRT–PCR primers. qRT–PCR primers were as follows. *Ccnd1* forward, 5′-GAGAAGTTGTGCATCTACACTG-3′; *Ccnd1* reverse, 5′-AAATGAACTTCACATCTGTGGC-3′; *Ccnd2* forward, 5′-CTACCGACTTCAAGTTTGCC-3′; *Ccnd2* reverse, 5′-GCTTTGAGACAATCCACATCAG-3′; *Cdk4* forward, 5′-AATGTTGTACGGCTGATGGA-3′; *Cdk4* reverse, 5′-AGAAACTGACGCATTAGATCCT-3′; *Cdk6* forward, 5′-GGCGTACCCACAGAAACCATA-3′; *Cdk6* reverse, 5′-AGGTAAGGGCCATCTGAAAACT-3′; *Ccnd3* forward, 5′-CGAGCCTCCTACTTCCAGTG-3′; *Ccnd3* reverse, 5′-GGACAGGTAGCGATCCAGGT-3′; *Rps6* forward, 5′-AGCTCCGCACCTTCTATGAGA-3′; *Rps6* reverse, 5′-GGGAAAACCTTGCTTGTCATTC-3′; *Rps21* forward, 5′-GTCCATCCAGATGAACGTGG-3′; *Rps21* reverse, 5′-CCATCAGCCTTAGCCAATCGG-3′.

31. El Marjou, F. *et al.* Tissue-specific and inducible Cre-mediated recombination in the gut epithelium. *Genesis* **39,** 186–193 (2004).
32. Barker, N. *et al.* Identification of stem cells in small intestine and colon by marker gene *Lgr5*. *Nature* **449,** 1003–1007 (2007).
33. Shibata, H. *et al.* Rapid colorectal adenoma formation initiated by conditional targeting of the *Apc* gene. *Science* **278,** 120–123 (1997).
34. Moser, A. R., Pitot, H. C. & Dove, W. F. A dominant mutation that predisposes to multiple intestinal neoplasia in the mouse. *Science* **247,** 322–324 (1990).
35. de Alboran, I. M. *et al.* Analysis of C-MYC function in normal cells via conditional gene-targeted mutation. *Immunity* **14,** 45–55 (2001).
36. Polak, P. *et al.* Adipose-specific knockout of raptor results in lean mice with enhanced mitochondrial respiration. *Cell Metab.* **8,** 399–410 (2008).
37. Luche, H., Weber, O., Nageswara Rao, T., Blum, C. & Fehling, H. J. Faithful activation of an extra-bright red fluorescent protein in "knock-in" Cre-reporter mice ideally suited for lineage tracing studies. *Eur. J. Immunol.* **37,** 43–53 (2007).
38. Tsukiyama-Kohara, K. *et al.* Adipose tissue reduction in mice lacking the translational inhibitor 4E-BP1. *Nature Med.* **7,** 1128–1132 (2001).
39. Banko, J. L. *et al.* The translation repressor 4E-BP2 is critical for eIF4F complex formation, synaptic plasticity, and memory in the hippocampus. *J. Neurosci.* **25,** 9581–9590 (2005).
40. Shima, H. *et al.* Disruption of the $p70^{s6k}$/$p85^{s6k}$ gene reveals a small mouse phenotype and a new functional S6 kinase. *EMBO J.* **17,** 6649–6659 (1998).
41. Ryazanov, A. G. Elongation factor-2 kinase and its newly discovered relatives. *FEBS Lett.* **514,** 26–29 (2002).
42. Ruvinsky, I. *et al.* Ribosomal protein S6 phosphorylation is a determinant of cell size and glucose homeostasis. *Genes Dev.* **19,** 2199–2211 (2005).

43. Sarbassov, D. D. *et al.* Prolonged rapamycin treatment inhibits mTORC2 assembly and Akt/PKB. *Mol. Cell* **22,** 159–168 (2006).

44. Sengupta, S., Peterson, T. R., Laplante, M., Oh, S. & Sabatini, D. M. mTORC1 controls fasting-induced ketogenesis and its modulation by ageing. *Nature* **468,** 1100–1104 (2010).

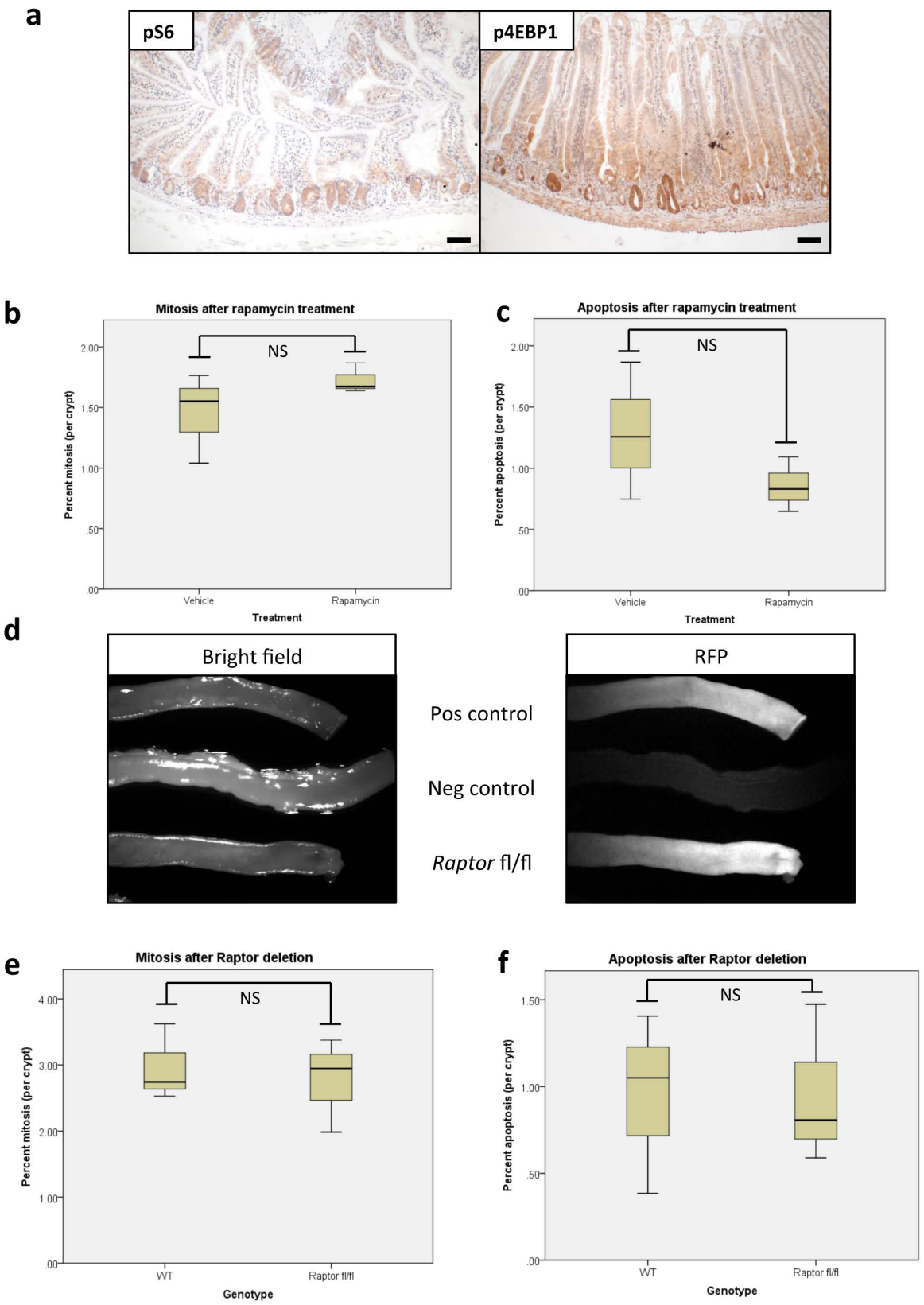

Extended Data Figure 1 | mTORC1 is activated following Wnt-signal and its inhibition does not affect homeostasis. **a**, Representative IHC of phospho-RPS6 (pS6) and phospho-4EBP1 (p4EBP1) show mTORC1 activity during intestinal regeneration, 72 h after 14 Gy γ-irradiation (representative of 5 biological replicates). **b**, **c**, Boxplots demonstrating that 72 h of 10 mg kg^{-1} rapamycin treatment does not alter mitosis or apoptosis in normal intestinal crypts. Whiskers show maximum and minimum, black line shows median ($n = 4$ per group). NS, not significant, Mann–Whitney *U* test. **d**, Intestines imaged on OV100 microscope, 96 h after induction, for red fluorescent protein (RFP). Tissue without the ROSA-tdRFP reporter (Neg control) show no RFP positivity, while the positive control (Pos control) and *Rptor*-deleted intestines show high RFP positivity (representative of 3 biological replicates). **e**, **f**, Boxplot showing that *Rptor* deletion does not affect mitosis or apoptosis rates in intestinal crypts, 96 h after induction. Whiskers show maximum and minimum, black line shows median ($n = 4$ per group). NS, not significant, Mann–Whitney *U* test. Scale bars, 100 μm.

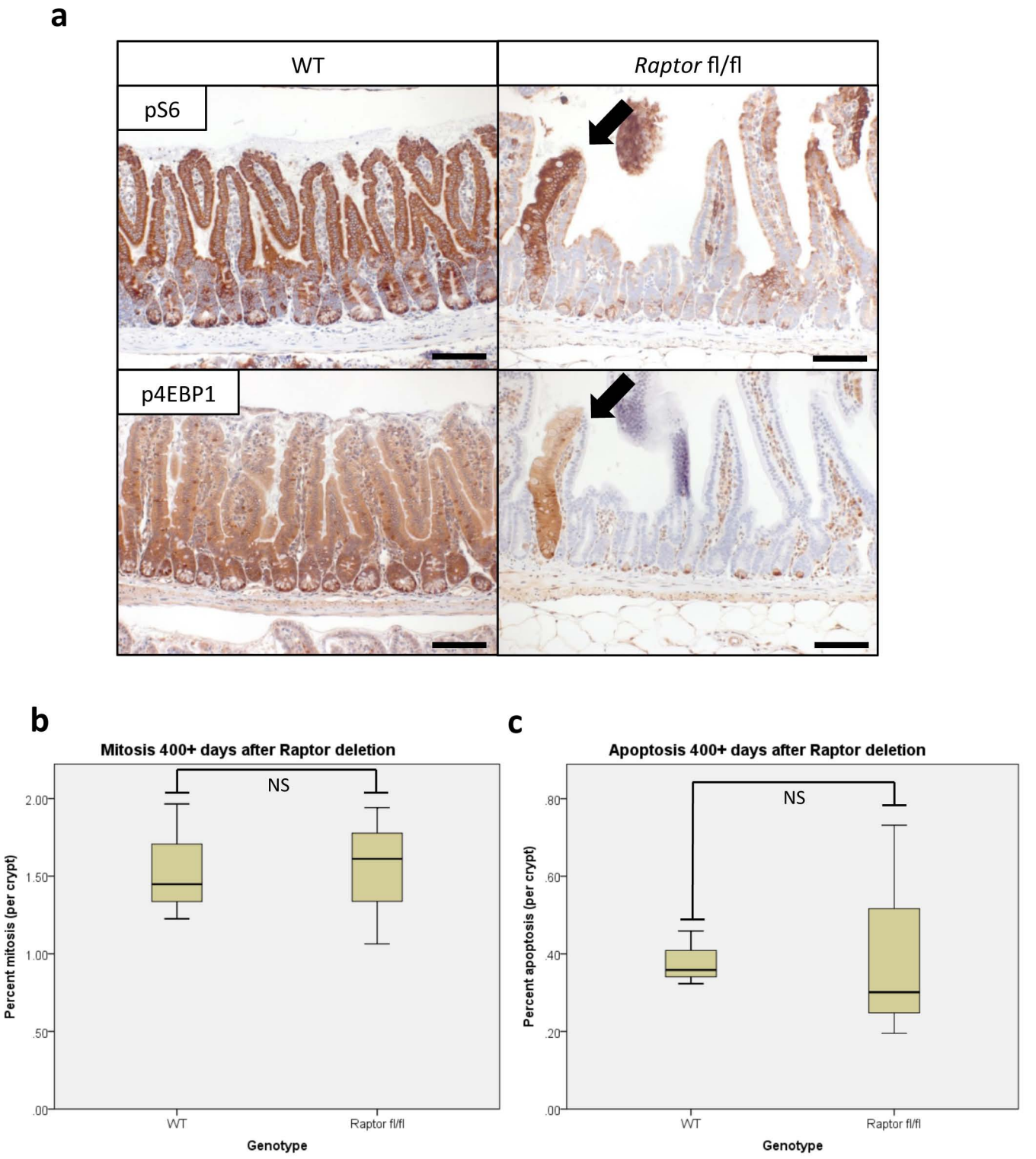

Extended Data Figure 2 | *Rptor* deletion is maintained in the small intestine. **a**, Representative IHC of phospho-RPS6 (pS6) and phospho-4EBP1 (p4EBP1) shows maintained loss of mTORC1 signalling 400+ days after *Rptor* deletion. Arrows indicate unrecombined escaper crypts that still show active mTORC1 signalling (representative of 5 biological replicates). **b**, **c**, Boxplots showing that mitosis and apoptosis are unchanged 400+ days after *Rptor* deletion. Mitosis and apoptosis were counted on H&E sections and are quantified as percent mitosis or apoptosis per crypt. Whiskers show maximum and minimum, black line shows median ($n = 5$ per group). NS, not significant, Mann–Whitney *U* test. Scale bars, 100 μm.

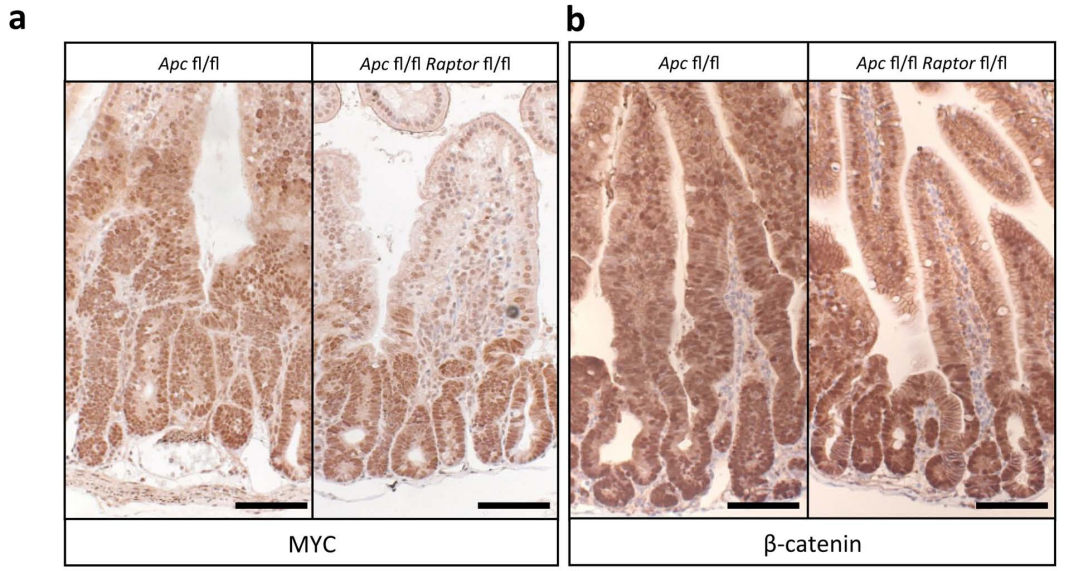

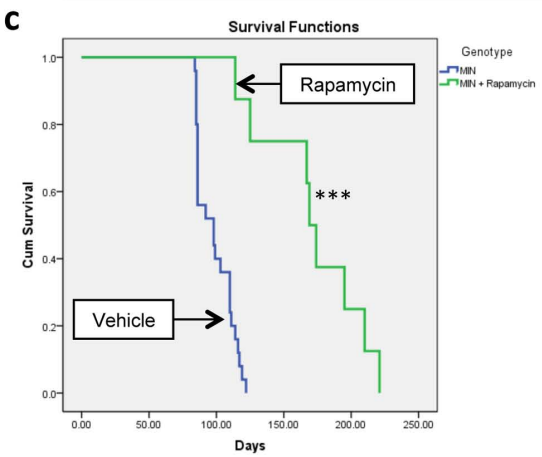

Apc Min/+	Median death
Vehicle	98
Rapamycin	169

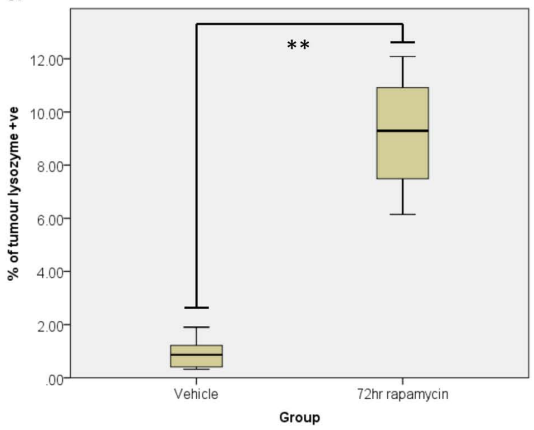

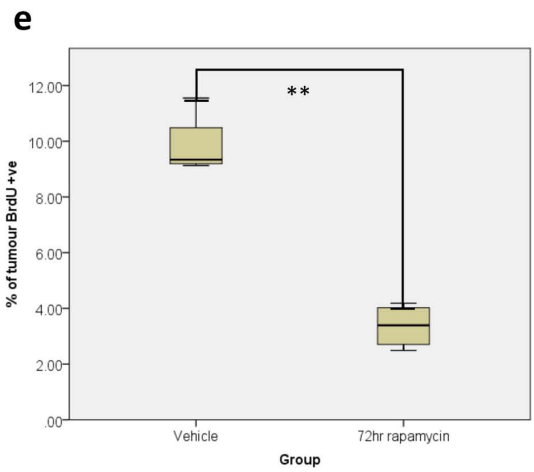

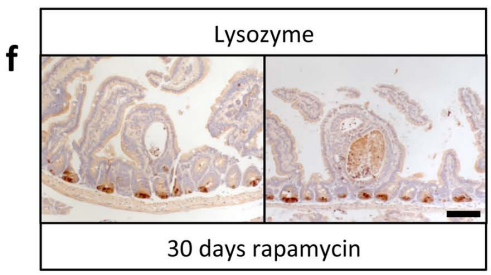

Extended Data Figure 3 | Wnt signalling is still active after *Rptor* deletion and rapamycin treatment causes regression of established tumours. **a**, **b**, Representative IHC of MYC and β-catenin showing high MYC levels and nuclear localization of β-catenin 96 h after *Apc* and *Apc/Rptor* deletion, demonstrating active Wnt signalling. Nuclear staining (as opposed to membranous staining) of β-catenin is indicative of active Wnt signalling. Scale bar, 100 μm (representative of 3 biological replicates). **c**, Kaplan–Meyer survival curve of $Apc^{Min/+}$ mice treated with rapamycin when showing signs of intestinal neoplasia. Rapamycin treatment (10 mg kg^{-1}) started when mice showed signs of intestinal disease, and was withdrawn after 30 days. Animals continued to be observed until signs of intestinal neoplasia. Death of animals in the rapamycin group almost always occurred after rapamycin withdrawal ($n = 8$ per group). ***P value ≤ 0.001, log-rank test. **d**, Boxplot showing that 72 h 10 mg kg^{-1} rapamycin treatment causes an increase in lysozyme-positive cells in tumours. Percentage lysozyme positivity within tumours was calculated using ImageJ software (http://imagej.nih.gov/ij/). Whiskers show maximum and minimum, black line shows median (10 tumours from each of 5 mice per group were measured. **P value ≤ 0.014, Mann–Whitney U test. **e**, Boxplot showing that 72 h 10 mg kg^{-1} rapamycin treatment causes a decrease in BrdU positivity within tumours. Percentage BrdU positivity within tumours was calculated using ImageJ software. Whiskers show maximum and minimum, black line shows median (10 tumours from each of 5 mice per group were measured). **P value ≤ 0.021, Mann–Whitney U test. **f**, Representative IHC of lysozyme, showing a lack of lysozyme-positive paneth cells in remaining cystic tumours after 30 days of 10 mg kg^{-1} rapamycin treatment. Scale bars, 100 μm (representative of 5 biological replicates).

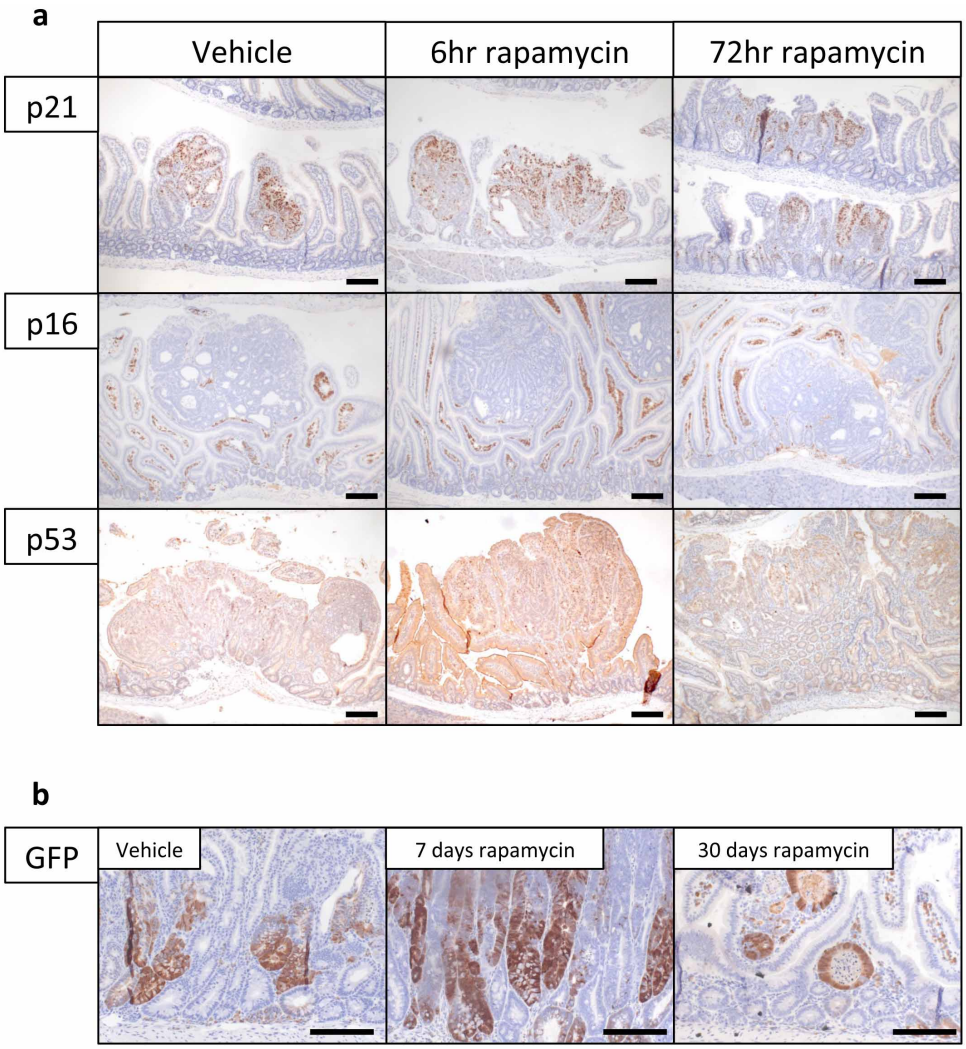

Extended Data Figure 4 | IHC after rapamycin treatment. **a**, Representative IHC of p21, p16 and p53 after 6 h and 72 h of 10 mg kg^{-1} rapamycin treatment. Staining shows no induction of these proteins in tumours after rapamycin treatment (representative of 5 biological replicates). **b**, Representative IHC for LGR5–GFP showing high numbers of LGR5-positive cells after 7 and 30 days of 10 mg kg^{-1} daily rapamycin treatment (representative of 5 biological replicates). Scale bars, 100 μm.

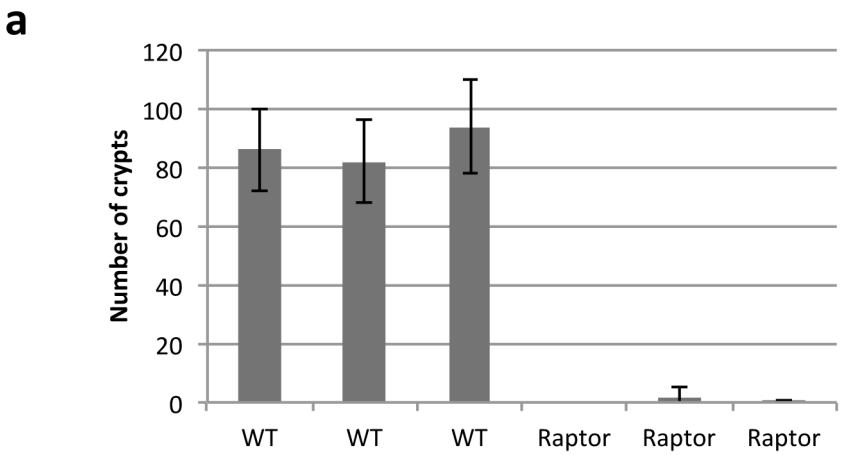

Extended Data Figure 5 | *Rptor* deletion in the intestinal crypt is lethal *in vitro*. **a**, Graph showing that *Rptor* deletion prevents intestinal crypts from growing *ex vivo*. Intestinal crypts were isolated and cultured as previously described[17], 96 h after *Cre* induction. Number of viable organoids was counted by eye 72 h after crypt isolation. WT, wild type. Data are average ± standard deviation ($n = 3$ biological replicates per group).

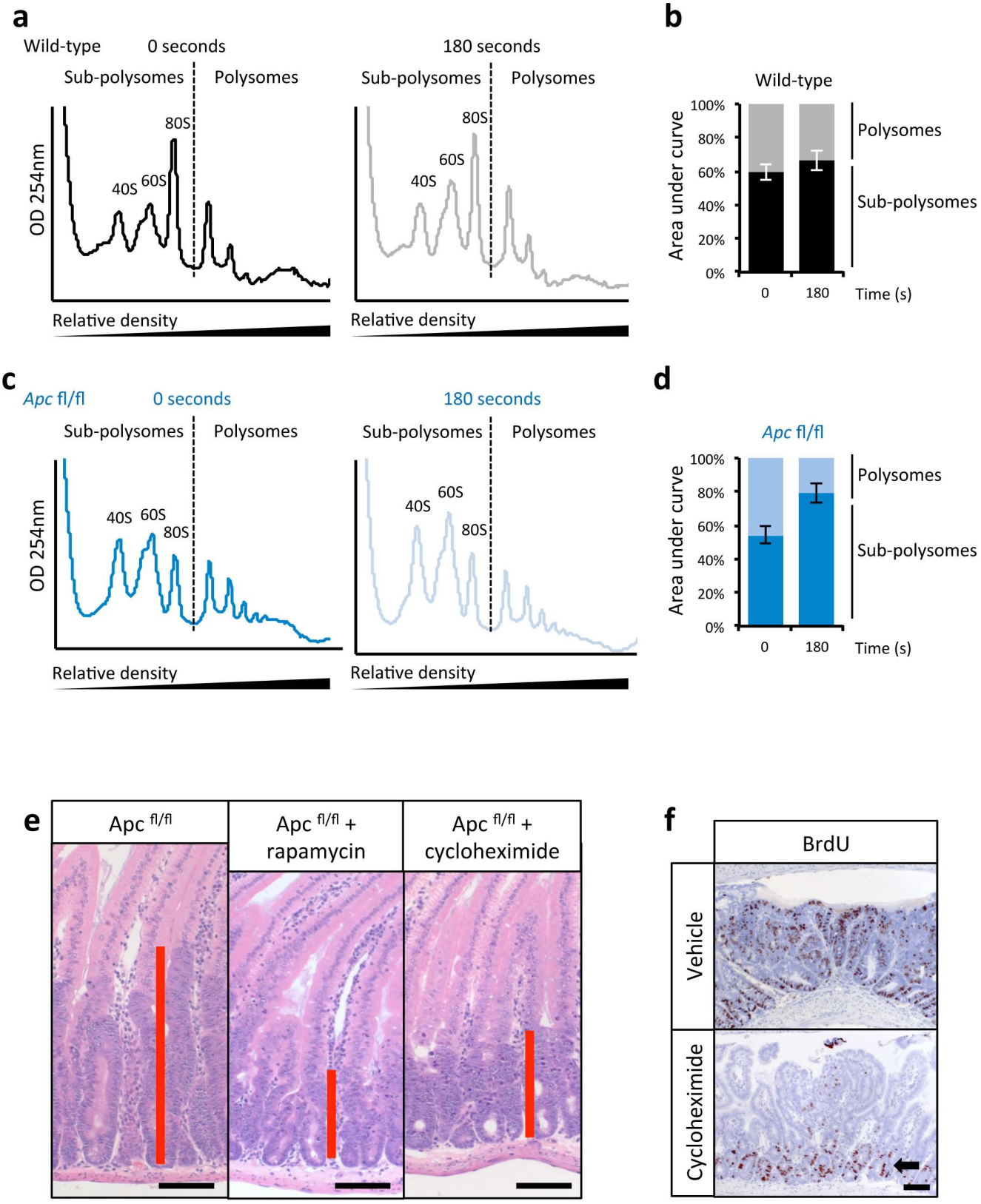

Extended Data Figure 6 | *Apc* deletion increases translational elongation rates and cycloheximide treatment phenocopies rapamycin treatment. **a**, Representative polysome profiles from wild-type *ex vivo* crypts incubated with harringtonine for 0 s (left) and 180 s (right) before harvest ($n = 3$ per time point). **b**, The areas under the sub-polysome (40S, 60S and 80S) and polysome sections as indicated by the dashed lines in **a** were quantified and expressed as a percentage of their sum. Data in the bar graph are the average ± s.e.m. ($n = 3$ per time point). **c**, **d**, Data are shown for *Apc*-deleted crypts, as for wild type in **b** and **c** ($n = 3$ biological replicates). **e**, Representative H&E staining showing that 35 mg kg^{-1} cycloheximide treatment phenocopies rapamycin treatment 96 h after *Apc* deletion. Treatment began 24 h after induction ($n = 3$ biological replicates). **f**, Representative IHC for BrdU showing a loss of proliferation in tumours after 72 h of 35 mg kg^{-1} cycloheximide treatment. ($n = 3$ biological replicates). Arrow highlights normal proliferating crypts. Scale bar, 100 μm.

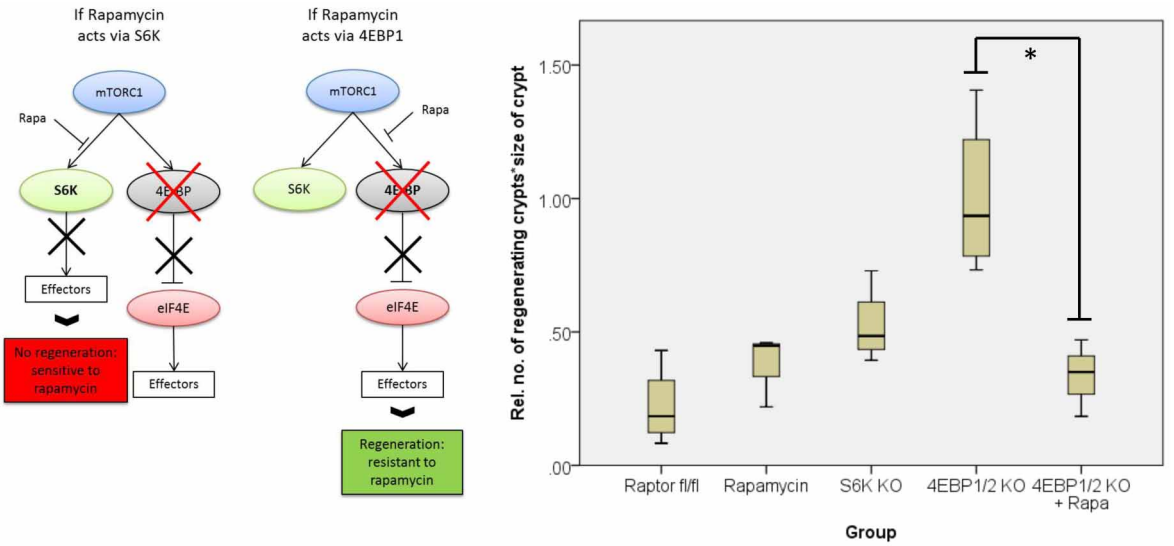

Extended Data Figure 7 | *S6k* deletion decreases intestinal regeneration. Graphical representation of findings, and boxplot showing that murine intestinal regeneration after irradiation is dependent on S6K. Animals were exposed to 14 Gy γ-irradiation, and intestinal regeneration was calculated 72 h after exposure by counting the number of viable crypts and multiplying that by the average size of the regenerating crypts. Relative regeneration was calculated by comparing each group to wild-type regeneration. The rapamycin treatment arm is reproduced from Fig. 4 for visual clarity. Whiskers show maximum and minimum, black line shows median ($n = 4$ per group). *P value = 0.034, Mann–Whitney U test.

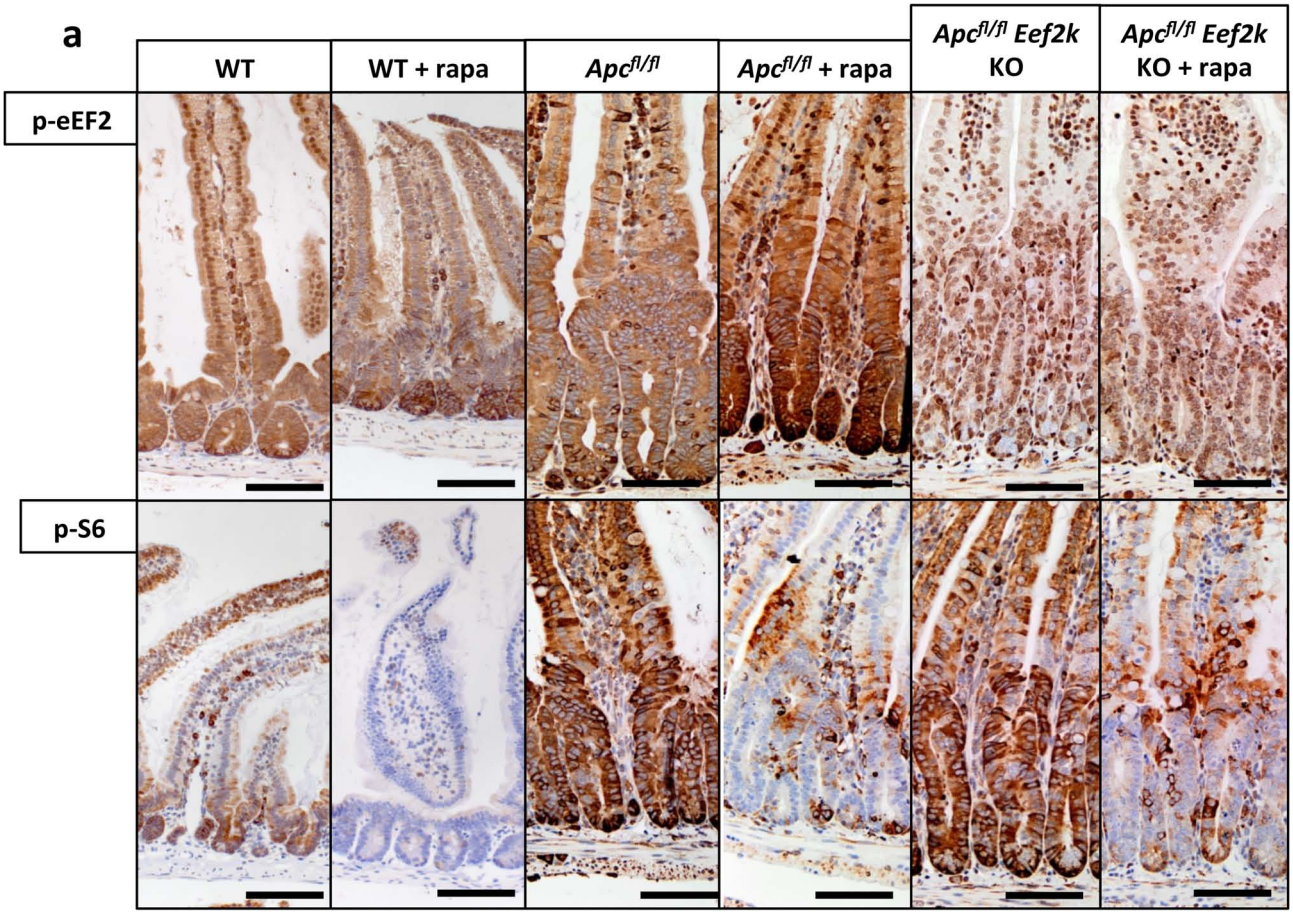

Extended Data Figure 8 | *Eef2k* deletion drives resistance to rapamycin. **a**, Representative IHC of phospho-eEF2 and phospho-RPS6 in wild-type (WT), *Apc*-deficient and *Apc*- and *Eef2k*-deficient mice (with or without 72 h 10 mg kg^{-1} rapamycin (rapa) treatment) shows that rapamycin is unable to induce eEF2 phosphorylation in the absence of eEF2K ($n = 6$ biological replicates). KO, knockout. Scale bars, 100 μm.

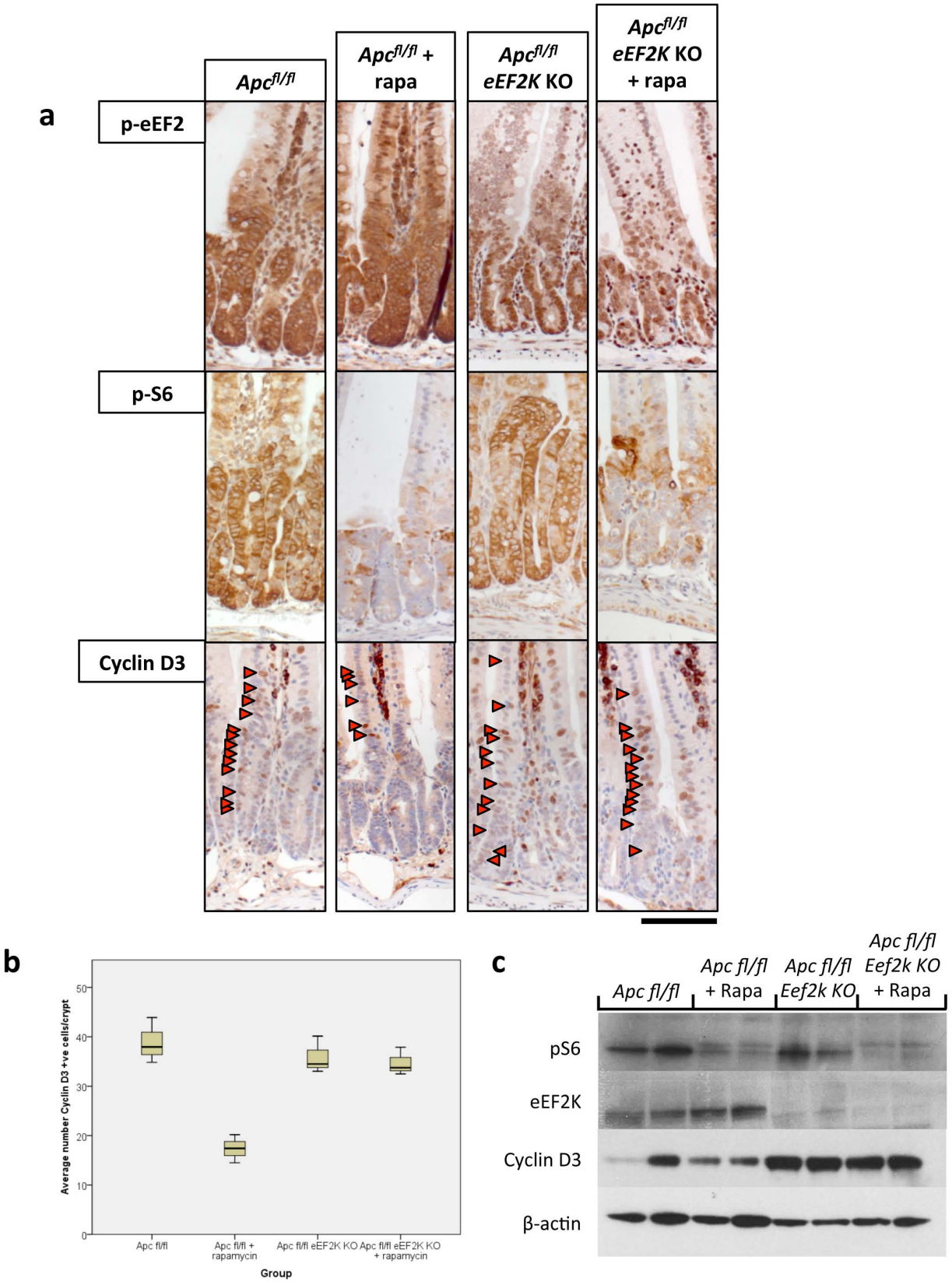

Extended Data Figure 9 | Cyclin D3 is regulated at the level of elongation. **a**, Representative IHC of *Apc*-deleted intestines with or without *Eef2k* deletion. Antibodies to eEF2K, phospho-RPS6 and cyclin D3 are shown (representative of 3 biological replicates). After *Eef2k* knockout (KO), cyclin D3 levels are no longer decreased upon 10 mg kg^{-1} rapamycin (rapa) treatment. **b**, Boxplot showing the number of cyclin-D3-positive cells per crypt, 96 h after *Apc* deletion, with and without 10 mg kg^{-1} rapamycin treatment. Graph shows that in *Eef2k* knockout animals, rapamycin no longer reduced cyclin D3 levels ($n = 3$ biological replicates per group). *P value ≤ 0.05, Mann–Whitney U test. **c**, Western blot analysis of intestinal epithelial cells from *Apc*-deleted and *Apc*-deleted *Eef2k* knockout, with and without 10 mg kg^{-1} rapamycin. Antibodies to eEF2K, phospho-RPS6, cyclin D3 and β-actin are shown. Each well represents a different mouse from the relevant group. Cyclin D3 levels are no longer reduced after *Eef2k* deletion. Scale bar, 100 μm.

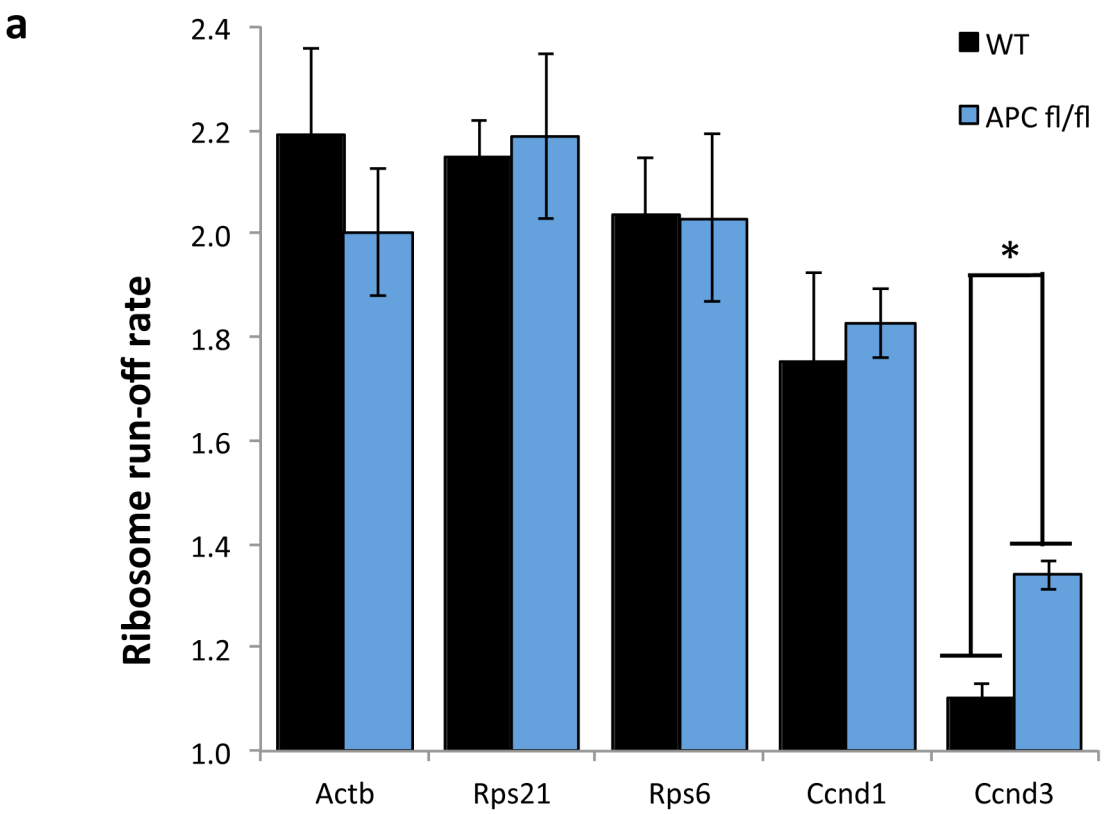

Extended Data Figure 10 | Ribosomes elongate faster on *Ccnd3* after *Apc* deletion. The ribosome run-off rate of various messages was measured as in Fig. 3. Elongation of *Ccnd3* was significantly increased, while *Actb*, *Rps21*, *Rps6* and *Ccnd1* remain unchanged. Data are average ± s.e.m. ($n = 3$ biological replicates per group). *P value ≤ 0.05, Mann–Whitney U test.